Resultant Deflections from Static Analysis of Sun Gear Rotor Shaft Materials to Determine Their Performance in 2-Stage Planetary Gear Operations

E. E. Mike*, I. A. Essienubong *‡

* Department of Production Engineering, University of Benin, Benin City, PMB 1154

(alwaysetuk@gmail.com, ikpeaniekan@gmail.com)

‡ Corresponding Author; Etuk Ekom Mike

ikpeaniekan@gmail.com

Abstract- This study evaluate the deflections undergone by four carbon steel materials applicable to statically loaded sun gear shaft in 2-stage planetary gear train. Using SOLIDWORKS 2018 version, Finite Element Method (FEM) was employed in modelling and analyzing the rotor sun gear shafts to determine the static nodal stresses, static displacement and static strain. The result revealed that Factor of Safety (FOS) significantly influence the level of failure as well as the strength possessed by the shaft material before failure. The analysis was carried out on the following materials: AISI 1020 Steel (cold rolled), cast carbon steel, cast carbon steel (cold rolled) and AISI 4130 steel (annealed at 865oC); with FOS of 13, 8.9, 9.1 and 15, and the strength possessed by each material before failure were observed as: 3.22e+08, 2.21e+08, 2.56e+08 and 4.31e+08 MPa. This indicates that AISI 4130 steel: annealed at 865oC is comparably the best among the four category of materials due to its very high FOS, followed by AISI 1020 Steel (cold rolled) and cast carbon steel (cold rolled). The von-Mises stress, resultant displacement and equivalent strain values produced were within the permissible limit, indicating that the four sun gear rotor shaft materials are suitable for application in 2-stage planetary gear operations and that the design is safe.

Keywords- Sun gear shaft, Static deflection, Carbon steel, Failure, Yield strength, FOS.

Özet- Bu çalışma, 2 kademeli planet dişli takımında statik olarak yüklenmiş güneş dişli miline uygulanabilen dört karbonlu çelik malzemeden kaynaklanan sapmaları değerlendirir. SOLIDWORKS 2018 versiyonunu kullanarak, statik düğüm gerilimlerini, statik yer değiştirme ve statik zorlamayı belirlemek için rotor güneş dişli millerinin modellenmesinde ve analizinde Sonlu Elemanlar Yöntemi (FEM) kullanılmıştır. Sonuç, Güvenlik Faktörünün (FOS) arıza seviyesini ve şafttan önce şaft malzemesinin sahip olduğu gücü önemli ölçüde etkilediğini ortaya koydu. Analiz şu malzemeler üzerinde gerçekleştirildi: AISI 1020 Çelik (soğuk haddelenmiş), dökme karbon çelik, dökme karbon çelik (soğuk haddelenmiş) ve AISI 4130 çelik (865oC'de tavlanmış); FOS 13, 8.9, 9.1 ve 15 ile ve her bir materyalin bozulmadan önce sahip olduğu kuvvet şu şekilde gözlendi: 3.22e + 08, 2.21e + 08, 2.56e + 08 ve 4.31e + 08 MPa. Bu, AISI 4130 çeliğinin: 865oC'de tavlanan, çok yüksek FOS nedeniyle dört malzeme kategorisi arasında nispeten en iyisi olduğunu, ardından AISI 1020 Çelik (soğuk haddelenmiş) ve dökme karbon çelik (soğuk haddelenmiş) olduğunu göstermektedir. Üretilen von-Mises gerilimi, ortaya çıkan yer değiştirme ve eşdeğer gerilme değerleri, dört güneş dişli rotor mili malzemesinin 2 kademeli planet dişli operasyonlarında uygulama için uygun olduğunu ve tasarımın güvenli olduğunu gösteren izin verilen sınırlar içerisindeydi.

Anahtar Kelimeler- Güneş dişli mili, Statik sapma, Karbon çeliği, Arıza, Akma dayanımı, FOS.

1. Introduction

Shaft is a term that relates to rotating machine members used in the transmission of power or torque. During machine operations where shaft is actively involved, it is subjected to loading conditions such as torsion, bending, and sometimes axial loading. In addition, stationary and rotating machine members, known as axles, carry rotating elements, and are

mainly subjected to bending loads. Shaft application can be classified into three major categories namely: transmission or line shafts which are relatively long shafts that transmit torque from motor to machine, countershafts which are short shafts between the driver motor and the driven machine and head shafts or stub shafts which are shafts directly connected to the motor [1, 2].

The Design and analysis of 125 mm shaft and rotor assembly for hammer mill crusher of capacity of 100 kg/hr, transmitting 20 B.H.P with a speed of 750 rpm using ANSYS software was carried out by Kumar [3]. The findings revealed that selecting a safety factor of 11 for the shaft diameter, shaft deflection of 0.009 mm was obtained theoretically by hand calculation while deflection of 0.007 mm was obtained by analysis using ANSYS software. Stress analysis on a turbine shaft was carried out by Ramakotaiah et al. [4] using conventional computer aided design tools. Bending stress computed based on the standard formulae with the help of computer C-program was 3.72 Mpa while bending stress computed using ANSYS 8.0 version was 3.55IMpa. Gujar and Bhaskar [5] investigated a rotor shaft in an inertia dynamometer rotated at 1000 rpm using FEM and theoretical approach. Logarithmic alternating/mean stress values were calculated theoretically as 7.2 Pa and 7.5 Pa which were less than the material alternating stress value of 7.94 Pa. Von-Mises stress value calculated by analytical approach was 38.26 N/mm2 while von-Mises stress value computed using FEM method was 33.20 N/mm2. Fatigue FOS was calculated theoretically was 1.72 while FEM computed FOS was 2.59. Rakesh et al. [6] employed both theoretical and FEM approach in the analysis of a 32 mm diameter shaft, fixed at one end and forces (5.4 KN at point A and 5.4 KN at point B) applied along the shaft. It was observed that the reactant forces acted in opposite directions while a torque of about 600 Nm acted at two points in opposite directions. The maximum shear stress value obtained theoretically was found to be 8.01 MPa while 8.09 MPa was obtained from the FEM approach using ANSYS 13.0 version. Eraslan and Akis [7] studied the plane strain and plane stress solutions of functionally graded rotating solid shaft and solid disk problems. Analytical solutions for the rotating solid shafts/disks were obtained by considering the nonlinear variation of the modulus of elasticity (E) in radial direction. Two different functions, one in exponential form and the other in parabolic form were used to describe the variation of E. The analysis indicated that at the centre of the shaft/disk, the stresses are finite, the radial and the circumferential stress components are equal and the values of the stresses are independent on the variation of the modulus of elasticity.

The application of finite element analysis is an established method for analysis that involves complex behaviour of high-speed rotator shafts under deformation and cross-section deformation. Moreover, analysis of rotor shafts with complicated geometries and varying sections or shafts experiencing large deformation is made to be less complicated when solid finite element method is employed [8]. Application of solid finite elements in analysing the dynamics of rotating members such as rotor shafts, however, can result in computational difficulties as a finite element model based on solid elements often consists of a very large number of degrees-of-freedom [9]. To overcome this limitation, a non-linear finite beam element formulation that uses cross-sectional discretization based on a continuum mechanics method was proposed by Yoon et al. [10]. The beam element was derived from three-dimensional solid elements, and the results obtained from the proposed method was acceptable for beams with complicated cross-section geometry under large twisting loading. Bozorgmehri et al. [11] employed a finite-element based absolute nodal coordinate formulation (ANCF) in dynamic analysis of high-speed rotating shafts. The objective was to study a four-node higher-order ANCF beam element with third-order derivatives in the axial and cross-section directions. From the numerical results, it was found that the higher-order ANCF beam can capture cross-section deformation and is therefore suitable for dynamic analysis on high speed-rotor shafts as well as the analysis of radial expansion in rotor shafts. Also for rotating shaft, it was added that the use of higher-order in transverse direction interpolation allows radial expansion and other cross deformation modes to be captured without requiring the use of computationally expensive solid elements. In this study, static deflection analysis was carried out on a sun gear rotor shaft to determine the performance of each shaft material applied in 2-stage planetary gear operation. The area of concern was to examine the nature of deflection on the shaft (in terms static stress, static displacement and static strain which constitutes to failure on the shaft when exposed to its in-service loading conditions) and to what end.

2. Materials and Methods

As shown in Figure 1a, modelling of the planetary gear/shaft assembly was done using SOLIDWORKS, 2018 version. Model of the rotary sun gear shaft is presented in Figure 1b. Four materials were selected from SOLIDWORKS material library for the analysis: AISI 1020 Steel (cold rolled), cast carbon steel (cold rolled), AISI 4130 steel (annealed at 865oC) and cast carbon steel. The aforementioned materials were selected on the basis of low cost and material properties (as shown in Table 1) suitable enough to sustain the shaft throughout its service life. To set up a deflection analysis in SOLIDWORKS simulation Environment, the loads and restraints on the model assembly must be defined first. As shown in Figure 1c, fixed hinge and fixed geometry type restraints (see Table 2 for the fixture details) were established at both ends of the shaft with concentrated loads (static loads were applied at top and mid-planes of the shaft) acting at the mid-planes of the shaft. Load details of the sun gear shaft are presented in Table 3. Gravity forces were also imposed in proper directions of the rotary sun gear shaft as shown in Table 3. The next step was to determine appropriate mesh for the study which was defined from the onset as deflection analysis. The study is based on Finite Element Method (FEM), and the mesh details as well as details of the study are presented in Table 4 while the visualized mesh on the sun gear shaft model is shown in Figure 2.
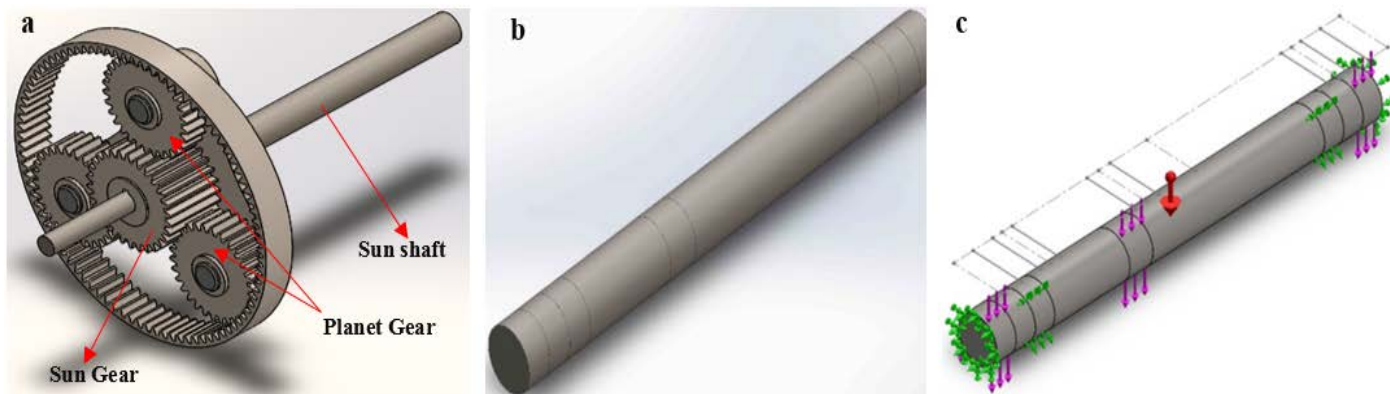
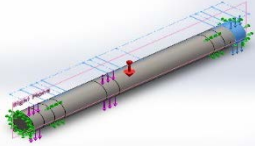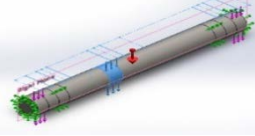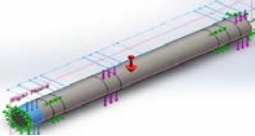**Fig. 1.** Planetary gear and sun gear shaft configuration model

Table 1. Properties of the sun gear shaft materials

Material Properties	AISI 1020 Steel, (Cold Rolled)	Cast Carbon Steel	Cast Carbon Steel (Cold Rolled)	AISI 4130 Steel (annealed at 865°C)
Yield strength	3.5e+008 N/m^2	2.48168e+08 N/m^2	2.84264e+08N/m^2	4.6e+08 N/m^2
Tensile strength	4.2e+008 N/m^2	4.82549e+08 N/m^2	4.82549e+08 N/m^2	5.6e+08 N/m^2
Elastic modulus	2.05e+011 N/m^2	2e+11 N/m^2	2e+11 N/m^2	2.05e+11 N/m^2
Poisson's ratio	0.29	0.32	0.32	0.285
Mass density	7870 kg/m^3	7800 kg/m^3	7820 kg/m^3	7850 kg/m^3
Shear modulus	8e+010 N/m^2	7.6e+10 N/m^2	7.6e+10 N/m^2	8e+10 N/m^2

Table 2. Fixture details for the static deflection analysis

Fixture Name	Fixture Details			
Fixed Hinge-1	Entities: 2 face(s) Type: Fixed Hinge			
Resultant Forces				
Components	X	Y	Z	Resultant
Reaction force(N)	-0.00871855	3066.52	0.220546	3066.52
Reaction Moment (N.m)	0	0	0	0
Fixture Name	**Fixture Details**			
Fixed-1	Entities: 2 face(s) Type: Fixed Geometry			
Resultant Forces				
Components	X	Y	Z	Resultant
Reaction force(N)	-0.0476986	734.3	-0.236036	734.3
Reaction Moment(N.m)	0	0	0	0

Table 3. Load details for the static deflection analysis

Load name	Load Images	Load Details	
Gravity-1		Reference	Top Plane
		Values	-9.81 m/s^2
Force-1		Entities	1 face(s), 1 plane(s)
		Reference	Right Plane
		Type	Apply force
		Values	-178 N
Force-2		Entities	1 face(s), 1 plane(s)
		Reference	Right Plane
		Type	Apply force
		Values	-2730.69 N
Force-3		Entities:	1 face(s), 1 plane(s)
		Reference:	Right Plane
		Type:	Apply force
		Values:	-853.306 N

Model name:Input Shaft22
Study name:Deflection Analysis(-Default-)
Mesh type: Solid Mesh

Fig 2. Mesh visualization of the sun gear shaft model

Table 4. Mesh and study details for the static deflection analysis

Mesh Details		Study Details	
Mesh Properties	Mesh Information	Study name	Deflection Analysis
Mesh type	Solid Mesh	Analysis type	Static
Mesher Used	Blended curvature-based mesh	Mesh type	Solid Mesh
Jacobian points	4 Points	Thermal Effect:	On
Maximum element size	5.86537 mm	Thermal option	Include temperature loads
Minimum element size	5.86537 mm	Zero strain temperature	298 Kelvin
Mesh Quality Plot	High	Solver type	FFEPlus
Total Nodes	29378	Inplane Effect:	Off
Total Elements	19352	Soft Spring:	Off
Maximum Aspect Ratio	3.3322	Inertial Relief:	Off
% of elements with Aspect Ratio < 3	100	Incompatible bonding options	Automatic
% of elements with Aspect Ratio > 10	0	Large displacement	Off

The planetary gears is keyed to the rotating sun gear shaft which rotates within a bearing. In the process of the shaft rotating about an axis, it is subjected to different loads including axial and radial induces stress that can translate into failure depending on the severity. The nature of stress to be considered in such case may be due to torque transmitted to the shaft, bending of the shaft due to its weight or load, and axial forces imparted to the shaft. For a rotor shaft transmitting power (Po) at a rotational speed (n), the transmitted torque T is given by Equation 1.

$$\left.\begin{array}{c} T\,(N-n) = 9550\,\frac{P_o(kW)}{n(rpm)} \\ or \\ T(in-Ib) = 63025\,\frac{P_o(hp)}{n(rpm)} \end{array}\right\} \quad (1)$$

The relation between nominal shear stress τ_{nom}, torque T, and polar-section modulus Zp is given by Equation 2.

$$\left.\begin{array}{c} \tau_{nom}(N/m^2) = \frac{T(N-m)}{Z_p(m^3)} \\ or \\ \tau_{nom}(Ib/in^2) = \frac{T(in-Ib)}{Z_p in^3} \end{array}\right\} \quad (2)$$

The nominal shear stress of the solid circular shaft with diameter (d) and hollowness factor (B) is given by

The nominal shear stress of the solid circular shaft with diameter (d) and hollowness factor (B) is given by Equation 3.

$$\tau_{nom} = \frac{16T}{\pi d_o^3} B \quad (3)$$

For a circular shaft with bending moment M and transverse section modulus Z, the nominal stress in bending is given by Equation 4.

$$\sigma_{nom} = \frac{32M}{\pi d_o^3} B \quad (4)$$

For a circular solid shaft subjected to static loading, the shaft deflection may result in stresses as well as minimum diameter (see Equation 5-7) according to distortion energy theory.

$$\sigma_b = \frac{M}{Z} = \frac{Mc}{I} = \frac{32M}{\pi d^3} \quad \{Bending\ Stress\} \quad (5)$$

$$\tau_T = \frac{T}{S} = \frac{Tc}{J} = \frac{16T}{\pi d^3} \quad \{Torsional\ Stress\} \quad (6)$$

$$d = \sqrt[3]{\frac{32fs}{\pi S_y} \sqrt{M^2 + \frac{3}{4}T^2}} \quad \left\{\begin{matrix} Minimum\ diameter \\ Distortion\ energy\ theory \end{matrix}\right\} (7)$$

were c is the maximum span, fs is factor of safety, I is the second moment of area, S is the polar section modulus, J is the second polar moment of area, Z is the section modulus and Sy is the yield strength. Considering the combined effect of torsion, bending, and axial loading on a circular shaft, if the shaft is subjected to torsion and bending, the stresses induced on the shaft are larger than the direct stress due to T and M alone. In that case, the effective nominal stress is given by Equation 8 [1].

$$\sigma_{ef} = \frac{32}{\pi d_o^3} B \left\{ \left[M + \frac{Fd_o}{8}(1+\alpha^2) \right]^2 + \frac{3}{4}T^2 \right\}^{1/2} \quad (8)$$

The alternating (a) and midrange (m) von-Mises stresses can be calculated using Equation 9a and 9b.

$$\sigma_a' = (\sigma_a^2 + 3\tau_a^2)^{1/2} \left[\left(\frac{32K_fM_a}{\pi d^3}\right)^2 + 3\left(\frac{16K_{fs}T_a}{\pi d^3}\right)^2 \right]^{1/2} \quad (9a)$$

$$\sigma_m' = (\sigma_m^2 + 3\tau_m^2)^{1/2} \left[\left(\frac{32K_fM_m}{\pi d^3}\right)^2 + 3\left(\frac{16K_{fs}T_m}{\pi d^3}\right)^2 \right]^{1/2} \quad (9b)$$

To check for yielding (ny) using von-Mises maximum stress, Equation 10 can be applied as follows:

$$n_y = \frac{S_y}{\sigma_{max}'} \quad (10)$$

$$\sigma_{max}' = [(\sigma_m + \sigma_a)^2 + 3(\tau_m + \tau_a)^2]^{1/2}$$

$$= \left[\left(\frac{32K_f(M_m+M_a)}{\pi d^3}\right)^2 + 3\left(\frac{16K_{fs}(T_m+T_a)}{\pi d^3}\right)^2 \right]^{1/2} \quad (11)$$

where Sy is the material yield strength. Each load case on the rotor shaft can be resolved as follows [12]:

$$Load = \sqrt{T^2 + M^2} \quad (12a)$$

$$Load = M \pm \frac{F*d}{8} \quad (12b)$$

$$Load = \sqrt{\left(\frac{F*d}{8}\right)^2 + T^2} \quad (12c)$$

$$Load = \sqrt{\left(M \pm \frac{F*d}{8}\right)^2 + T^2} \quad (12d)$$

Equation 12a is applicable when torque (T) and bending moment (M) are present. When bending moment and axial force are present, the load case can be expressed using Equation 12b (F is positive, if it produces tension stress and negative, if it produces compression stress). Equation 12c is applicable when torque and axial force are present while Equation 12d can be used for calculating load cases that involves torque, bending moment and axial force. Failure occurs when the effective stress σ_{ef} exceeds the yield strength of the material σ_y. Thus, for ductile metals where local yielding at stress concentration is acceptable, the shaft diameter is given by Equation 13 [1].

$$d_o^3 = \frac{FS}{\sigma_y}\frac{32}{\pi} B \left\{ \left[M + \frac{Fd_o}{8}(1+\alpha^2) \right]^2 + \frac{3}{4}T^2 \right\}^{1/2} \quad (13)$$

Were FS is the design Factor of Safety and F is the axial force. The diameter of shafts made from brittle materials can be expressed as:

$$d_o^3 = \frac{FS}{\sigma_u}\frac{32}{\pi} B \left\{ \left[(K_t)_b M + (K_t)_a \frac{Fd_o}{8}(1+\alpha^2) \right]^2 + \frac{3}{4}[(K_t)_t T]^2 \right\}^{1/2} (14)$$

where $(K_t)_b$ is the theoretical stress factor in bending, $(K_t)_a$ is the theoretical stress factor in axial loading and $(K_t)_t$ is the theoretical stress factor in torsion. According to the energy distortion theory, when both the bending and torsional moments acting on the shaft are fluctuating, the safe diameter for the shaft is expressed as:

$$d_o^3 = \frac{32(FS)}{\pi} B \left[\left(\frac{M_m}{\sigma_u} + \frac{M_a}{\sigma_f} \right)^2 + \frac{3}{4}\left(\frac{T_m}{\sigma_y} + \frac{T_a}{\sigma_{f,t}} \right)^2 \right]^{\frac{1}{2}} \quad (15)$$

were Ma is the alternating bending moment, Mm is the steady bending moment, Ta is the alternating torque and is the steady torque. In the case of fluctuating torsional load that consist of an alternating torque Ta superimposed on a steady torque Tm, the shaft diameter can be expressed as:

$$d^3 = \frac{16(FS)}{\pi} \left(\frac{T_a}{\tau_f} + \frac{T_m}{\tau_U} \right) \quad (16)$$

were τ_f is the reversed torsional fatigue limit and τ_U is the ultimate shear strength. To avoid possible yielding failure, the shaft diameter should not be smaller than:

$$d^3 = \frac{16\sqrt{3}}{\pi}(FS)\left(\frac{T_a+T_m}{\sigma_y} \right) \quad (17)$$

Kinetic energy of the rotor shaft model is expressed as the sum of the translational kinetic energy of its centroidal line and the rotational kinetic energy of its cross sections. Therefore, the

kinetic energy of any part of the rotating shaft is given by Equation 18 [13].

$$T = \frac{1}{2}\iiint \rho\ \dot{r}.\dot{r}dx\ dy\ dz = \frac{1}{2}\iiint \rho\ [(\dot{u}^2 + \dot{v}^2 + \dot{w}^2) + \Omega^2(u^2 + v^2) + 2\Omega^2(yv + xu) + 2\Omega(u\dot{v} - v\dot{u}) + \Omega^2(x^2 + y^2) + 2\Omega(x\dot{v} - y\dot{u})]dxdydz \quad (18)$$

where p is the shaft density, Ω is the rotating speed of the shaft, u, v, w are the flexural displacements of any point on the cross-section of the shaft in the x, y, and z directions, dx, dy and dz are the z are the position vectors. Since small displacements are assumed in the rotating reference frame, the potential energy (V) of the concerned part of the shaft cm be given by Equation 19 [14].

$$V = \frac{E}{2(1+v)}\iiint \left[\frac{v}{1-2v}\left(\frac{\partial u}{\partial x} + \frac{\partial v}{\partial y} + \frac{\partial w}{\partial z}\right)^2 + \left(\frac{\partial u}{\partial x}\right)^2 + \left(\frac{\partial v}{\partial y}\right)^2 + \left(\frac{\partial w}{\partial z}\right)^2 + \frac{1}{2}\left(\frac{\partial w}{\partial y} + \frac{\partial v}{\partial z}\right)^2 + \frac{1}{2}\left(\frac{\partial u}{\partial z} + \frac{\partial w}{\partial x}\right)^2 + \frac{1}{2}\left(\frac{\partial v}{\partial x} + \frac{\partial u}{\partial y}\right)^2 \right] dx\ dy\ dz \quad (19)$$

The displacement functions u(ξ, η, ζ), v(ξ, η, ζ) and w(ξ, η, ζ) can be interpolated in terms of nodal variables. For the three-dimensional elasticity problem, partial differentiation is carried out with respect to global coordinates x, y, z. From the following local coordinates (ξ, η, ζ,), the Jacobian matrix [J] is introduced based on the rules of partial differentiation [15].

$$\{P_l\} = [J]\{P_g\} \quad (20a)$$

Where,

$$\{P_l\} = \begin{Bmatrix} \frac{\partial}{\partial \xi} \\ \frac{\partial}{\partial \eta} \\ \frac{\partial}{\partial \zeta} \end{Bmatrix}, \quad \{P_g\} = \begin{Bmatrix} \frac{\partial}{\partial x} \\ \frac{\partial}{\partial y} \\ \frac{\partial}{\partial x} \end{Bmatrix}, \quad [J] = \begin{Bmatrix} \frac{\partial x}{\partial \xi} & \frac{\partial y}{\partial \xi} & \frac{z}{\xi} \\ \frac{\partial x}{\partial \eta} & \frac{\partial y}{\partial \eta} & \frac{\partial z}{\partial \eta} \\ \frac{\partial x}{\partial \zeta} & \frac{\partial y}{\partial \zeta} & \frac{\partial z}{\partial \zeta} \end{Bmatrix} \quad (21b)$$

The matrix [J] can be given explicitly in terms of the local coordinates as:

$$[J] = \begin{Bmatrix} \frac{\partial\{g\}^T}{\partial \xi} \\ \frac{\partial\{g\}^T}{\partial \eta} \\ \frac{\partial\{g\}^T}{\partial \zeta} \end{Bmatrix} [T]^{-1} [\{x_i\}\ \{y_i\}\ \{z_i\}] \quad (22)$$

For the strain matrices, there are six strain components relevant in full three-dimensional elasticity analysis given as:

$$\{\varepsilon\} = \begin{Bmatrix} \varepsilon_x \\ \varepsilon_y \\ \varepsilon_z \\ \varepsilon_{xy} \\ \varepsilon_{yz} \\ \varepsilon_{zx} \end{Bmatrix} = \begin{Bmatrix} \frac{\partial u}{\partial x} \\ \frac{\partial v}{\partial y} \\ \frac{\partial w}{\partial z} \\ \frac{\partial u}{\partial y} + \frac{\partial v}{\partial x} \\ \frac{\partial v}{\partial z} + \frac{\partial w}{\partial y} \\ \frac{\partial u}{\partial z} + \frac{\partial w}{\partial x} \end{Bmatrix} = [B]\begin{bmatrix} \{P_g\} & 0 & 0 \\ 0 & \{P_g\} & 0 \\ 0 & 0 & \{P_g\} \end{bmatrix} (23)$$

3. Results and Discussion

Design Factor of Safety (FOS) otherwise known as safety factor is the ratio of a component's absolute strength to actual applied load. In other words, it is the measure of how reliable a particular design component is [16]. From the colour band or legend representing the plot for FOS in Figures 3a-d, red colour which is at the bottom of the colour band indicates the minimum FOS with which the rotor sun gear shaft should be based. A low Factor of Safety implies that with further additional load, the material will exceed its elastic region and result in permanent deformation [17]. Other colours like orange and yellow which are ascending from the bottom of the colour band indicates an increasing order of the FOS. Lemon and green colours are observed to be at the mid-range in the colour band which represents an increasing order in the shaft design FOS. From the colour band, sky blue and aqua (SVG) also indicate further increase in the design FOS but royal blue which is at the top of the colour band and the highest FOS that the rotor sun gear shaft design can be based. It can be observed in the colour band for the FOS plots representing all the materials in this study that royal blue colour which signifies the maximum design FOS for the rotor shaft design is designated by number Fifteen (15). It should be noted in the FOS plots for all simulated rotor sun gear shaft models in this study, that royal blue colour signifies minimum severity in terms of failure while the red colour signifies maximum severity in terms of failure. This connotes the findings of Etuk et al. [18] where FEM was also employed in analysing FOS in relation to 2-stage planetary gear for horizontal axis wind turbine. From engineering point of view, the higher the FOS value selected for a given design, the higher the performance of the component in terms of strength and resistance against its in-service loading condition. However, this often goes at a cost, as higher FOS implies better manufacturing techniques, durable and expensive materials which all result in high material yield strength, improved service performance and longevity as well as high cost in the price of finished product [19]. From the FOS simulated plots for the following rotor sun gear shaft materials, AISI 1020 Steel (cold rolled), cast carbon steel, cast carbon steel (cold rolled) and AISI 4130 steel (annealed at 865oC), FOS of 13, 8.9, 9.1 and 15 were obtained as shown on the upper left hand corner of the simulated plot in Figures 3a-d. This implies that, sun gear shaft material with the highest FOS which in this case is AISI 4130 steel: annealed at 865oC should exhibit the highest strength before failure, lowest resultant displacement and lowest equivalent strain. This will be verified in subsequent plots simulated for the aforementioned parameters.
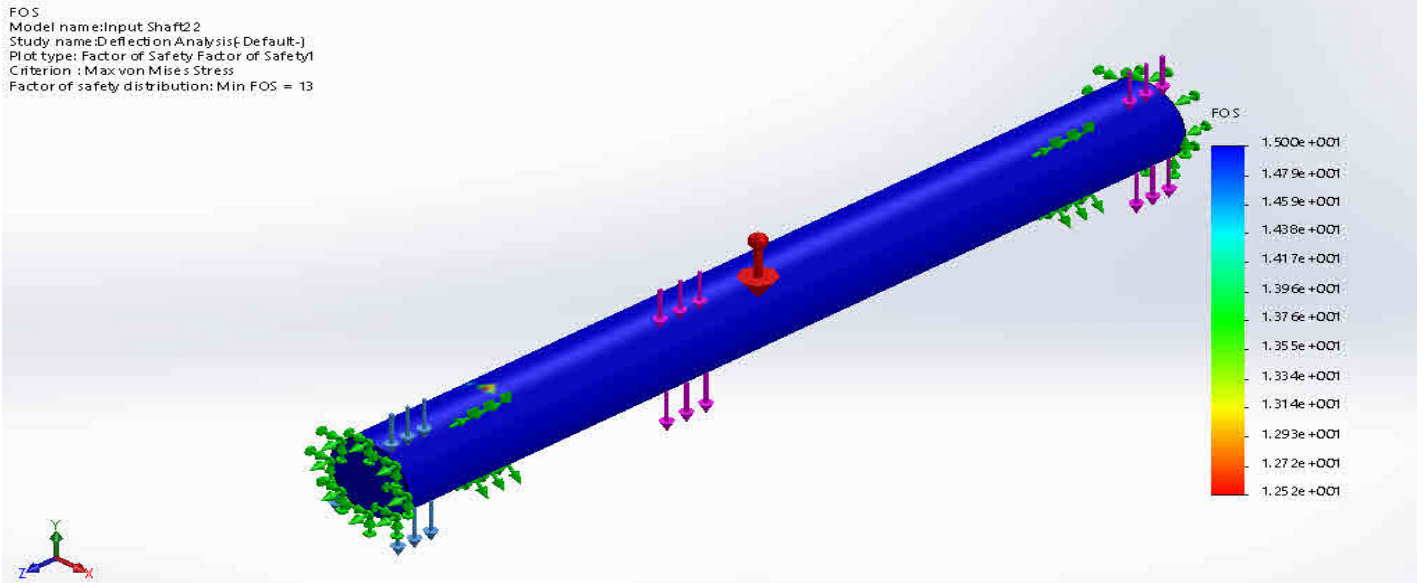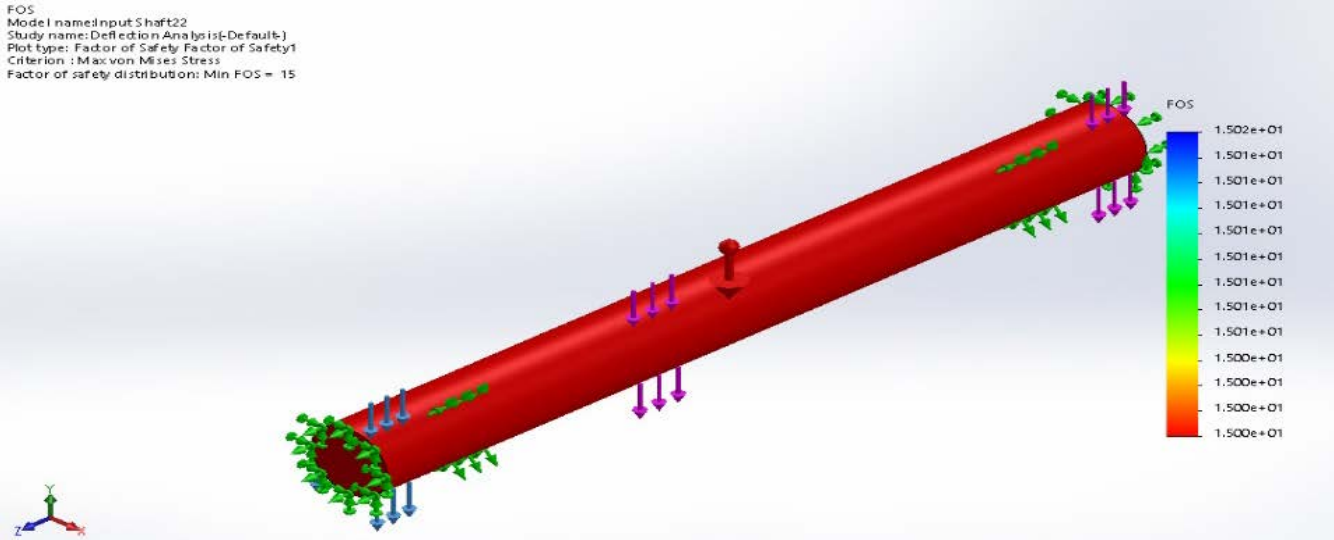
Fig 3a. Factor of safety simulation plot for AISI 1020 Steel (cold rolled)
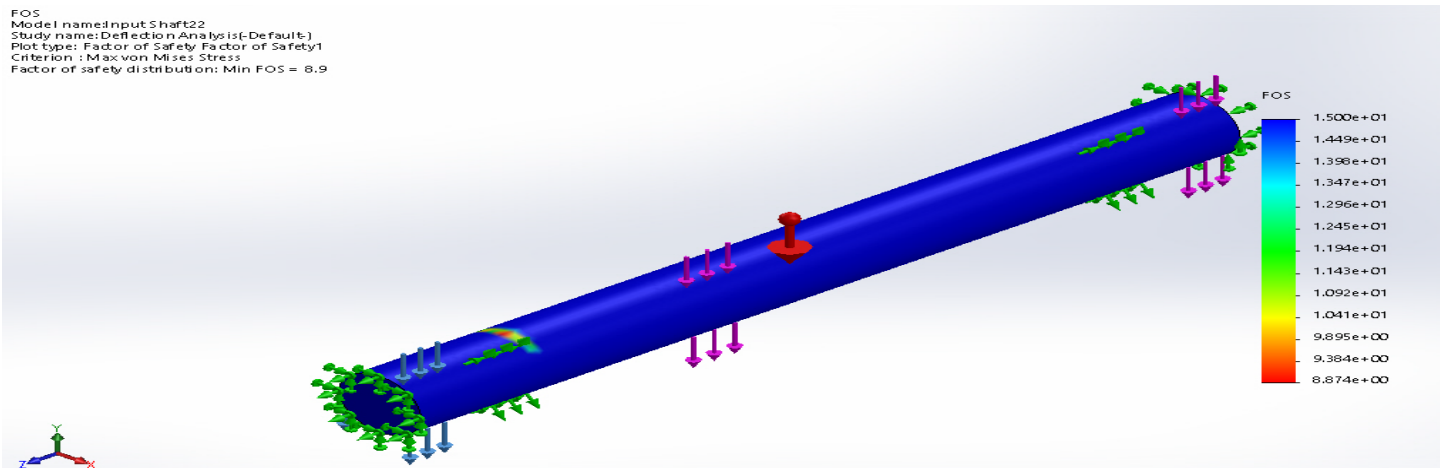
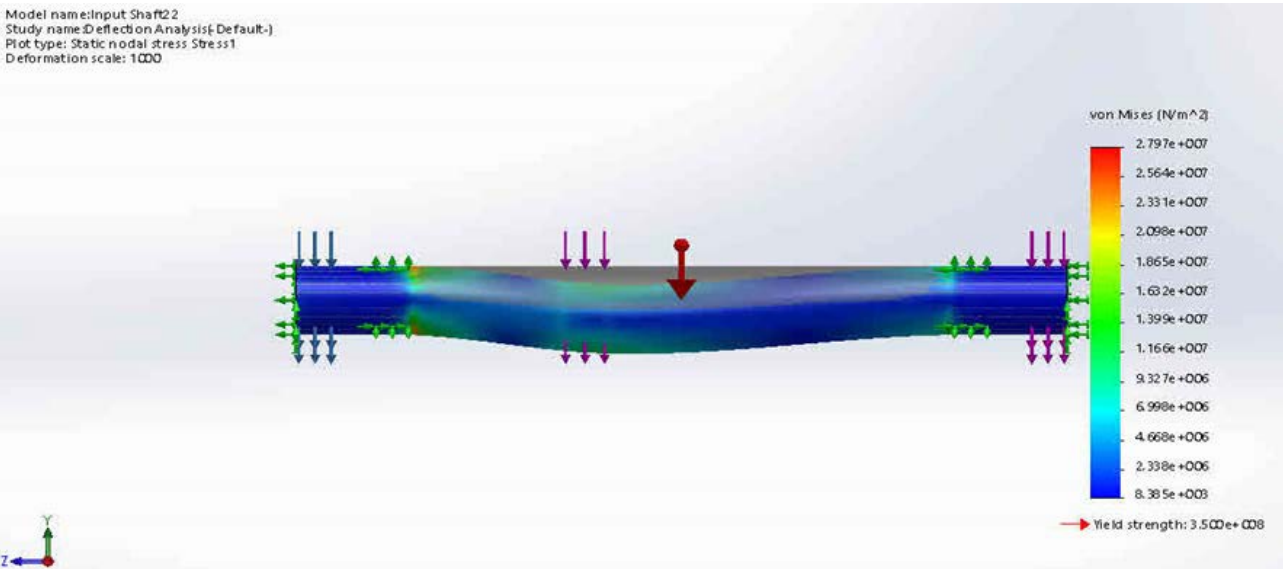**Fig 3b**. Factor of safety simulation plot for cast carbon Steel
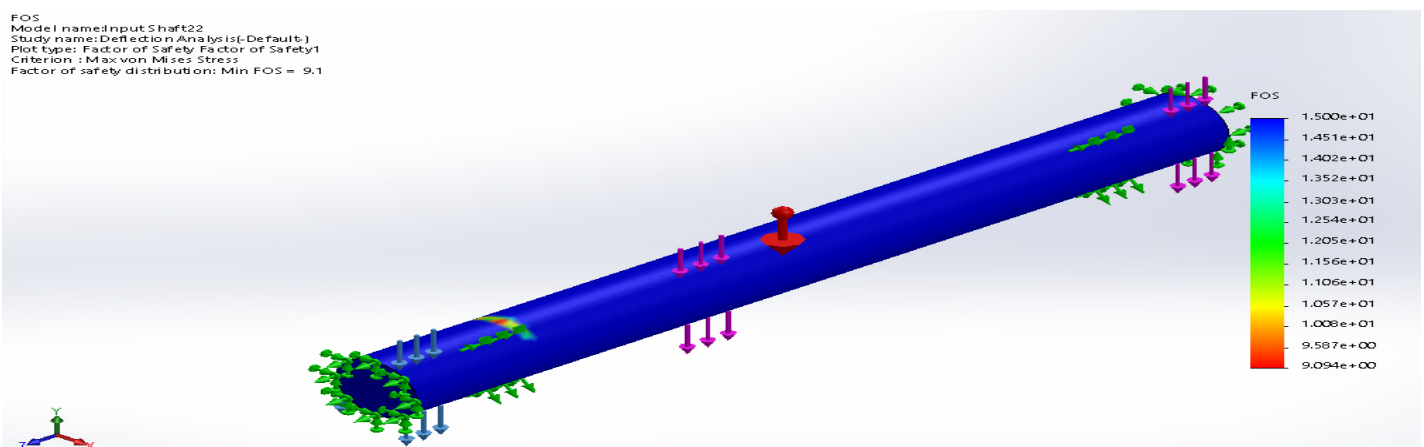
Fig 3c. Factor of safety simulation plot for cast carbon steel (cold rolled)

Fig 3d. Factor of safety simulation plot for AISI 4130 steel, annealed at 865oC

Shaft deflections are calculated using simply supported beam equations Ryan [20], but the level of accuracy may not be as high as deflections calculated from computational methods such as FEM. The rotor sun gear shaft was modelled as a beam with simple supports at both ends and concentrated loads acting at its mid-planes, and the deflections acting along the shaft length was determined. The shaft deflection in this case is observed on the output plot where the deflected model is characterized by different colors corresponding to the numerical results which are also associated with the color bands. Areas of high stresses, high resultant displacement and high equivalent strain indicates unsafe zones which are prone to the highest level of deformation and vice versa [21, 22], and can be identified using the color band or legend on the simulated plots presented in Figures 4a-d. Red color which is at the top of the color band indicates the area with maximum stress concentration, on the shaft material, followed by orange color, light green color, green color and so on. On the other hand, royal blue which is at the bottom of the color band indicates safe zones as well as the areas with minimum stress concertation on the shaft material. Sky blue indicates the stress level at which the shaft material begins to respond to the applied load, aqua (SVG) blue indicates further stress level from sky blue color [23, 24]. The color band representing the von-Mises stress, resultant displacement and equivalent strain plot is the reverse of the color band representing the plots of engineering Factor of Safety (FOS) for the same materials in this study.

Fig 4a. Static nodal stress simulation plot for AISI 1020 steel (cold rolled)
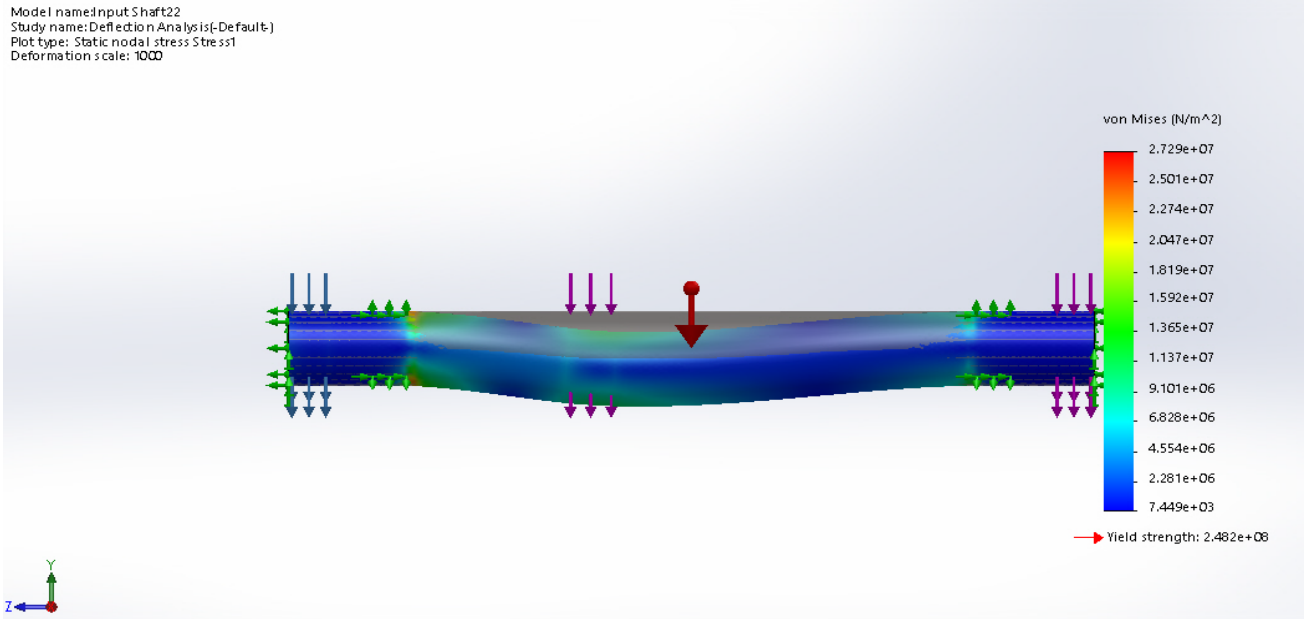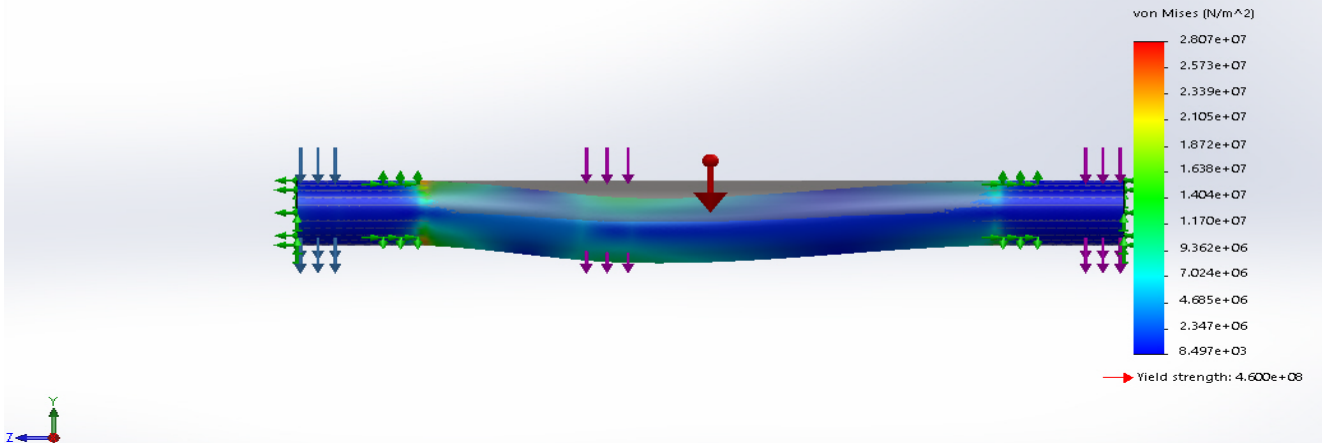
Fig 4b. Static nodal stress simulation plot for cast carbon steel
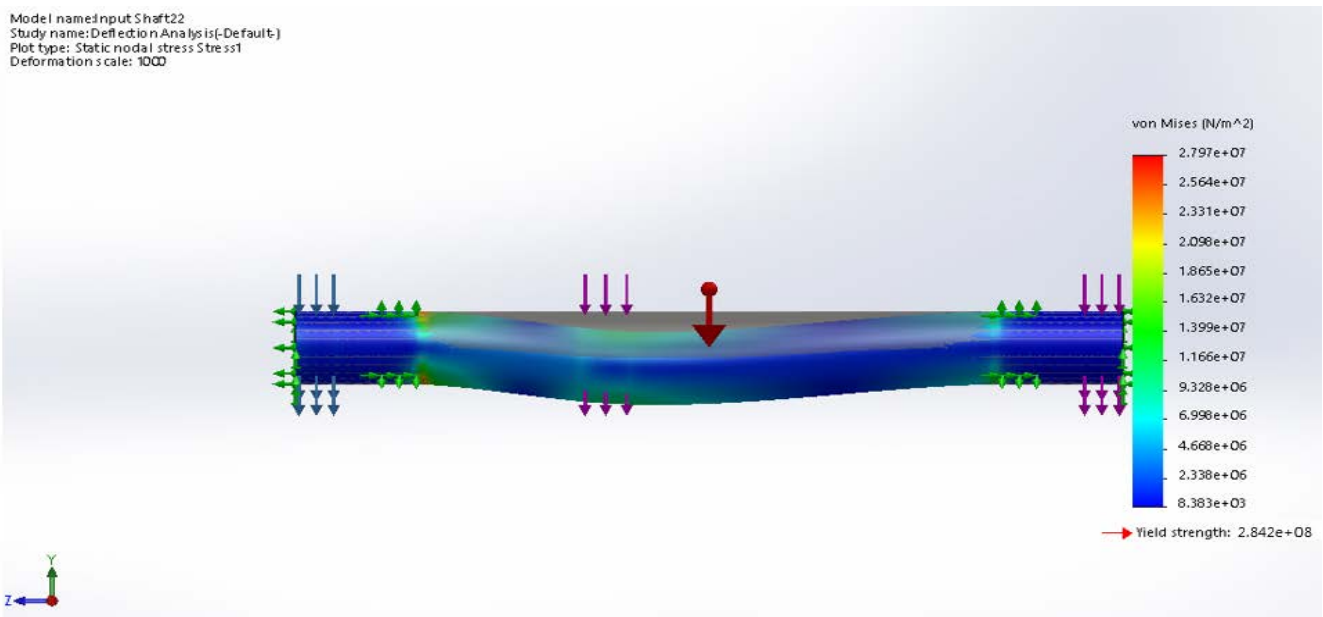
**Fig 4c.** Static nodal stress simulation plot for cast carbon steel (cold rolled)

Fig 4d. Static nodal stress simulation plot for AISI 4130 steel, annealed at $865^o C$

Considering von-Mises failure theory, material component is said to be in a state of failure if the von-Mises stress exceeds the material yield strength, but if the von-Mises stress value is less than the material's yield strength, the material is considered to be safe. This relates to the theory behind elasticity of materials which state that the material can take additional load provided its elastic limit is not exceeded [25, 26]. For clarity and understanding, maximum von-Mises stresses for each rotor sun gear shaft material as well as their respective yield strength were extracted from the simulated static nodal stress plot in Figures 4a-d and presented as shown in Figure 5. Considering the maximum von-Mises stresses and yield strength obtained for each sun gear shaft material, it can be observed that the maximum von-mises stress values of all the four (4) materials were below their yield strength, indicating that all the for materials in this study considered are good choice of materials that can withstand the in-service loading condition of a rotor sun gear shaft in 2-stage planetary gear application without untimely failure.
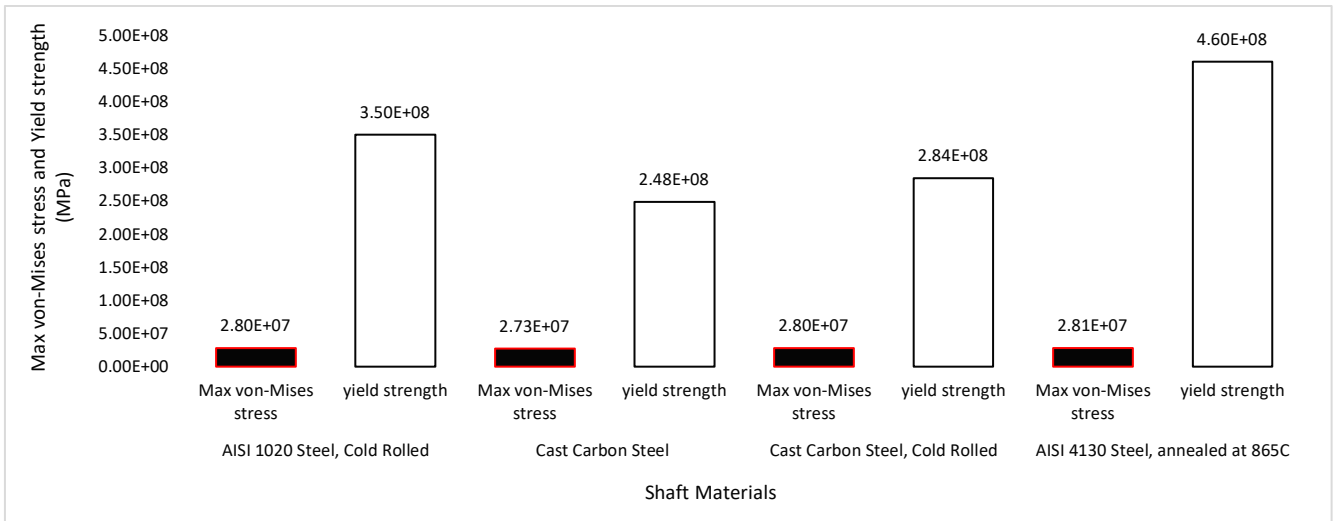
Fig 5. Graphical representation of von-Mises stress and yield strength

Considering that failure is inevitable in engineering components, it is necessary to determine how much strength that each of the rotor sun gear shaft material has before failure. To achieve that, the maximum von-Mises stress for each shaft material considered in this study was subtracted from its yield strength and the difference were plotted (see Figure 6) as the total strength (MPa) possess by each shaft material in its service life under normal operating condition before failure. It can be observed in Figure 6, that AISI 4130 steel (annealed at 865oC) possessed the highest strength before exceeding the its

yield strength or before failure, followed by AISI 1020 steel (cold rolled), cast carbon steel (cold rolled) and cast carbon steel. The plot in Figure 6 also confirms that FOS of a given material also plays a vital role to its service performance in terms of strength and durability, as AISI 4130 steel (annealed at 865oC) which possessed the highest strength before failure also had the highest FOS, followed by AISI 1020 steel (cold rolled), cast carbon steel (cold rolled) and cast carbon steel.
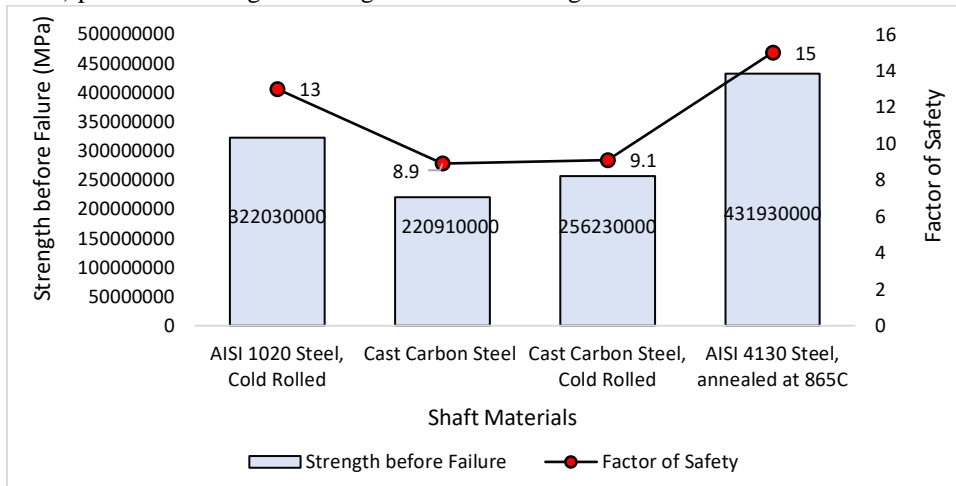

Fig 6. Graphical representation of material strength before failure and FOS

Static displacement is the deflection of body under quasi-static load. That is, the load is applied slowly, such that no significant inertia loads are developed. In this case, the rotor sun gear shaft is exposed to bending from its initial position under the influence of point load at its centre, axial or radial forces at both ends during its service condition. Therefore, the slope of the said deflected shaft may be described as the angle between its initial position and the deflected position. From the finite element plots obtained from the simulation of rotor

sun gear shaft in 2-stage planetary gear, it can be observed in Figures 7a-d that maximum displacement from its original position due to the forces acting on it, occurred at the mid-plane of the shaft while minimum displacement occurred at both ends. This therefore implies that the free ends of the rotor sun gear shaft are constrained to electric motor or pulley while the mid-plane which is constrained to the sun gear is subjected to the forces transmitted by the gear and its rotating members.
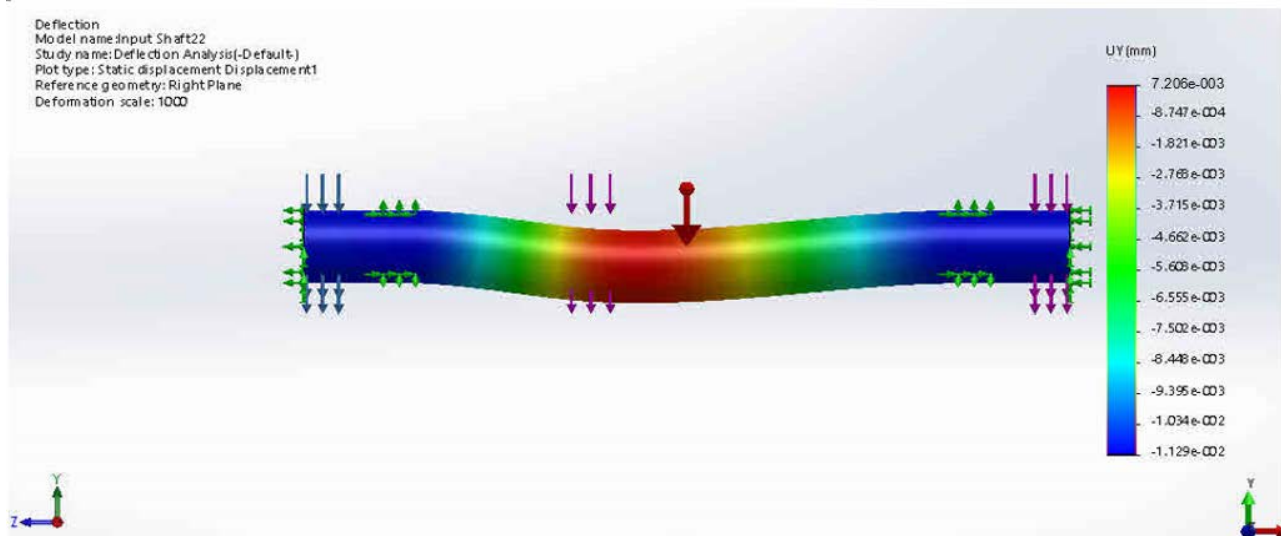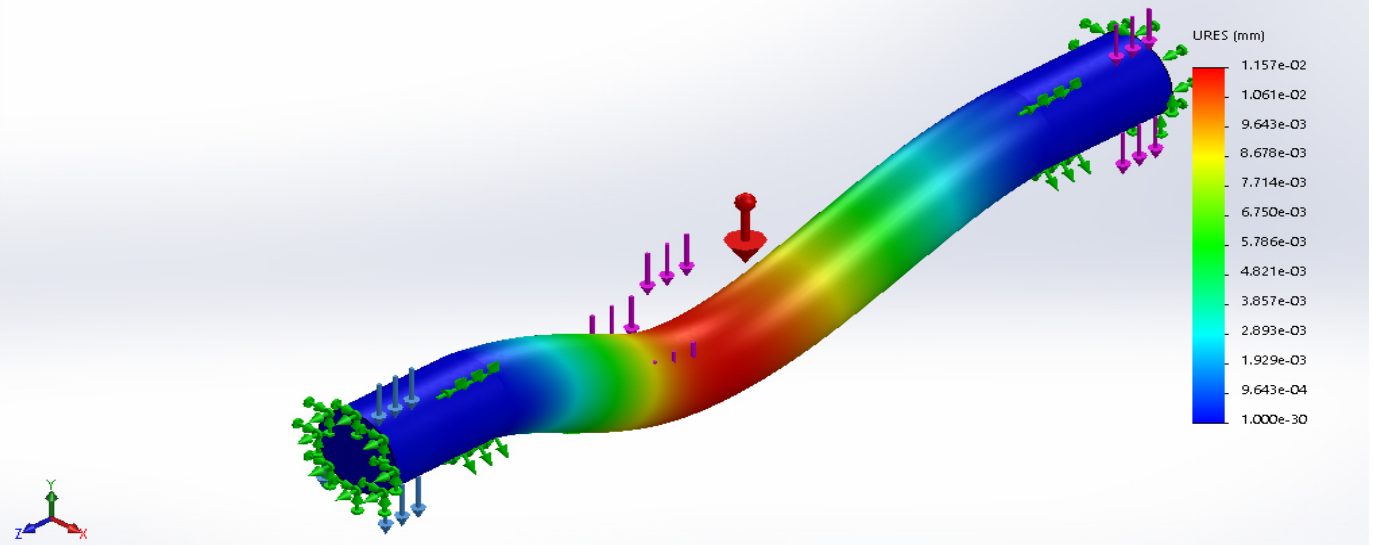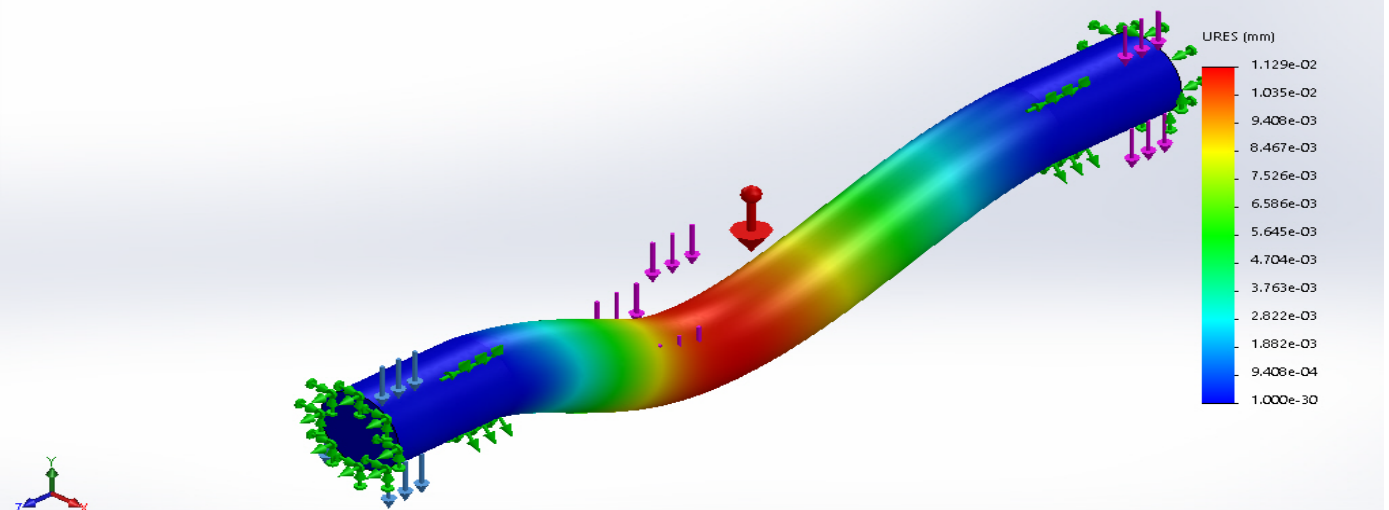

Fig 7a. Static displacement simulation plot for AISI 1020 steel (cold rolled)

Model name:Input Shaft22
Study name:Deflection Analysis(-Default-)
Plot type: Static displacement Displacement2
Deformation scale: 3456.9

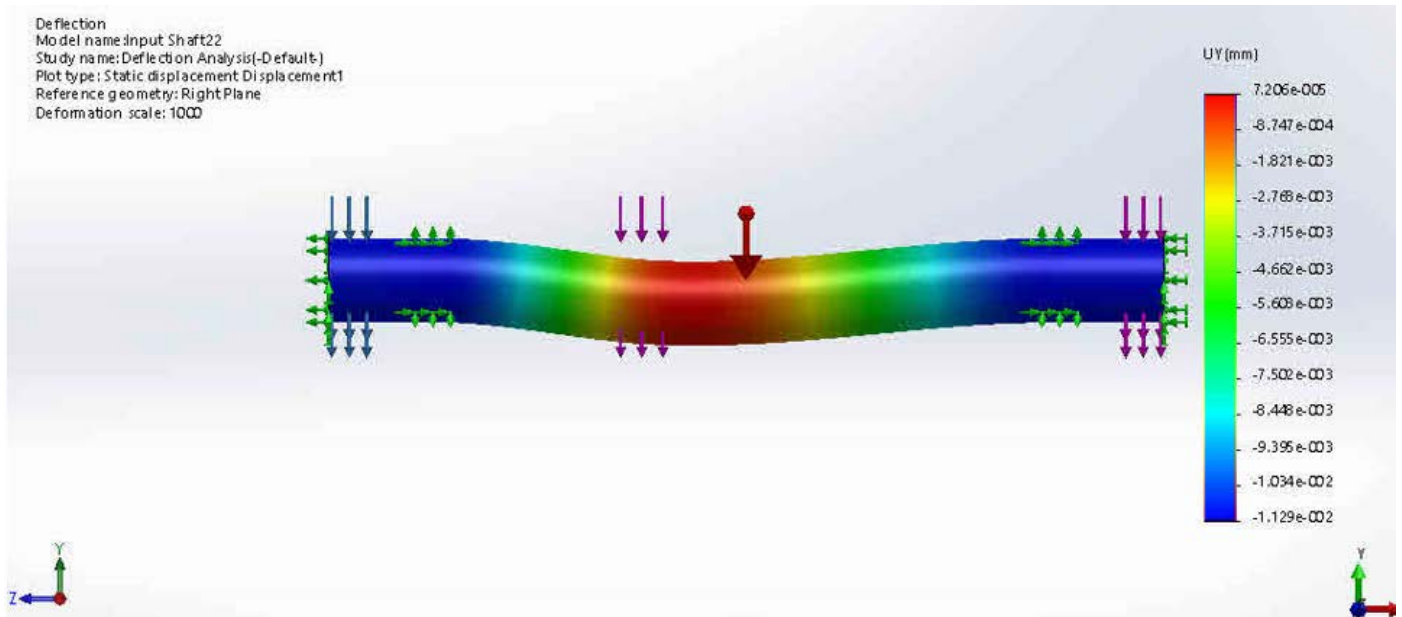**Fig 7b.** Static displacement simulation plot for cast carbon steel

Model name:Input Shaft22
Study name:Deflection Analysis(-Default-)
Plot type: Static displacement Displacement2
Deformation scale: 3543.1

Fig 7c. Static displacement simulation plot for cast carbon steel (cold rolled)

Fig 7d. Static displacement simulation plot for AISI 4130 steel, annealed at $865^{o}C$

Maximum resultant displacement on each rotor sun gear shaft material extracted from the simulated plot in Figures 7a-d indicated that AISI 4130 steel (annealed at 865oC) possessed the minimum level of displacement, followed by AISI 1020 steel (cold rolled), cast carbon steel (cold rolled) before cast carbon steel. Considering the failure implication of this, it implies that rotor sun gear shaft design with cast carbon steel will be the first to fail, followed by cast carbon steel (cold rolled) while AISI 4130 steel (annealed at 865oC) will be the last to give way. As observed in Figure 8, this therefore imply that a given shaft material with high FOS will undergo less displacement and may not fail untimely during service condition and vice versa.
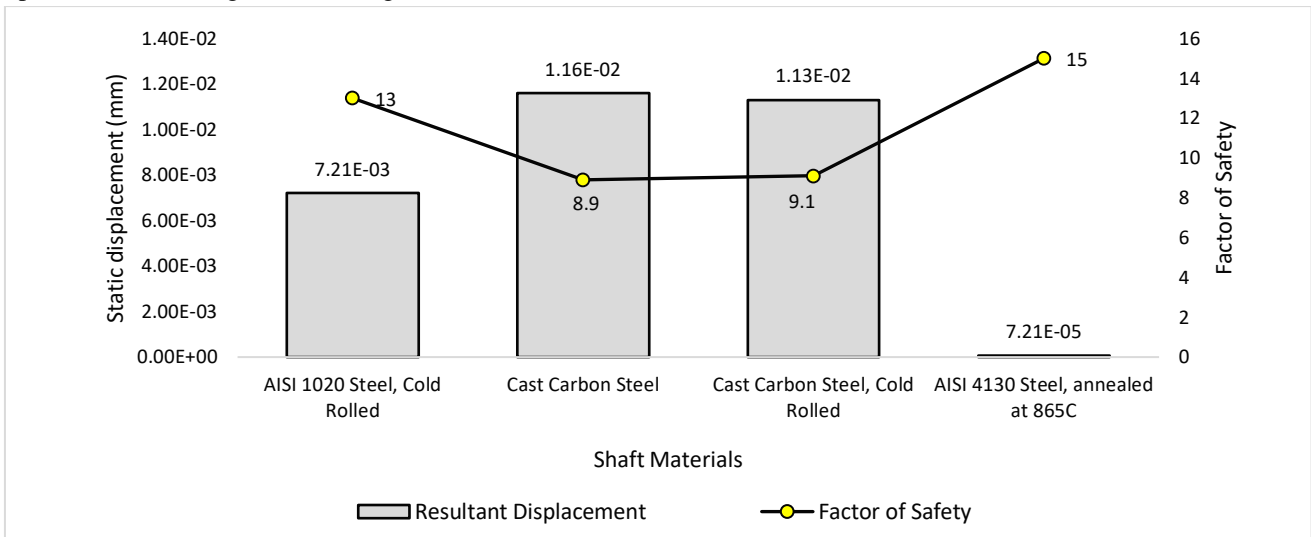
Fig 8. Graphical representation of static displace on the sun gear shaft and FOS

Strain is the ratio of change in deformation undergone by an object in response to the applied load or force to its original length [17]. The type of strain associated with the rotor sun gear shaft in this study is the shear strain which is the length of deformation on the shaft divided by the perpendicular length in the plane of the applied force. Strain is an important property of ductile materials, as they are designed to obey Hook's law which states that: "within the elastic limit of a ductile material, the deformation (strain) produced by the applied force is proportional to the force". Therefore, if the material's elastic limit is not exceeded, the material returns to its original shape and size after the force is removed, otherwise, it remains permanently deformed or stretched. The force at which the material exceeds its elastic limit is called

limit of proportionality [27]. Based on plasticity theory, when load is applied on components designed with ductile material, it results in plastic deformation which occurs evenly across constrained regions of the material, and may continue as the load increases [28]. The tensile deformation is followed by necking which indicate the areas where relatively large amount of strain localize disproportionately in a small region of the material component prior to its failure [29]. The static strain simulation of the rotor sun gear shaft was performed using a deformation scale of 1 as the threshold. Carefully observing the rotor sun gear shaft simulated plot in Figures 9a-d, it can be observed that maximum static strains resulting from applied loads on each of the rotor sun gear shaft material have not exceeded and are not even closer to the threshold, indicating that it is almost impossible for the sun gear shaft materials to fail under the influence of shear strain.
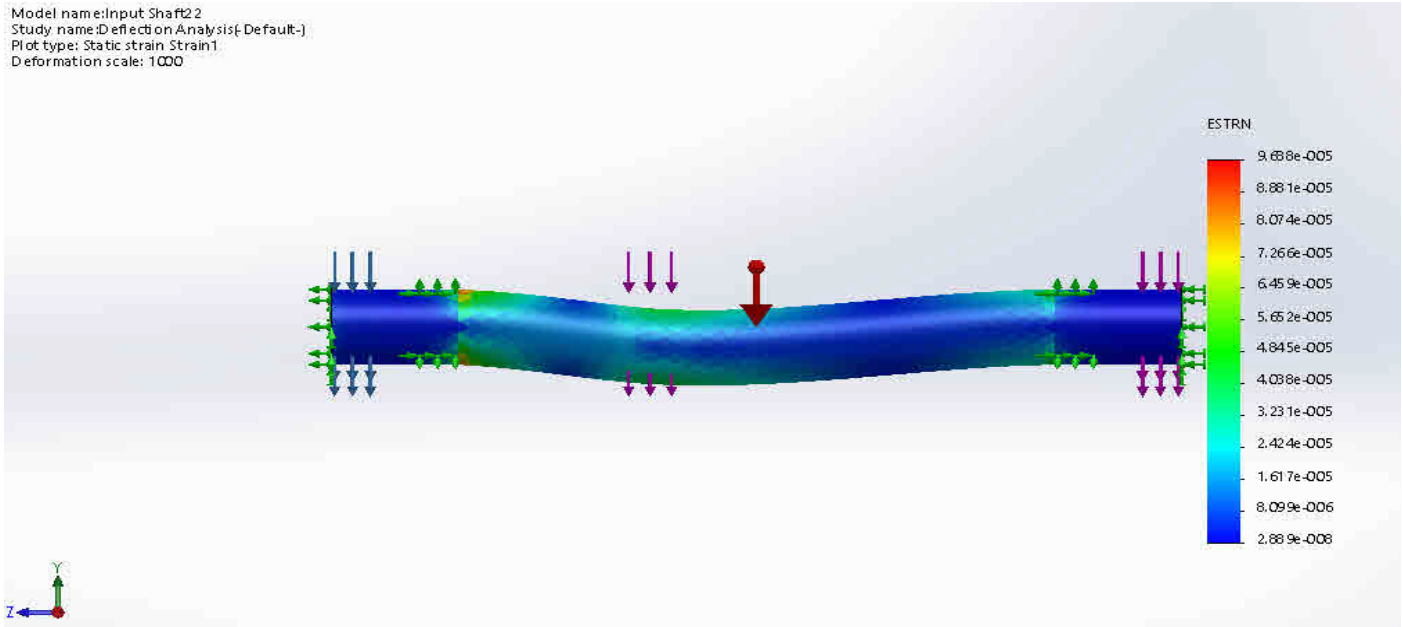

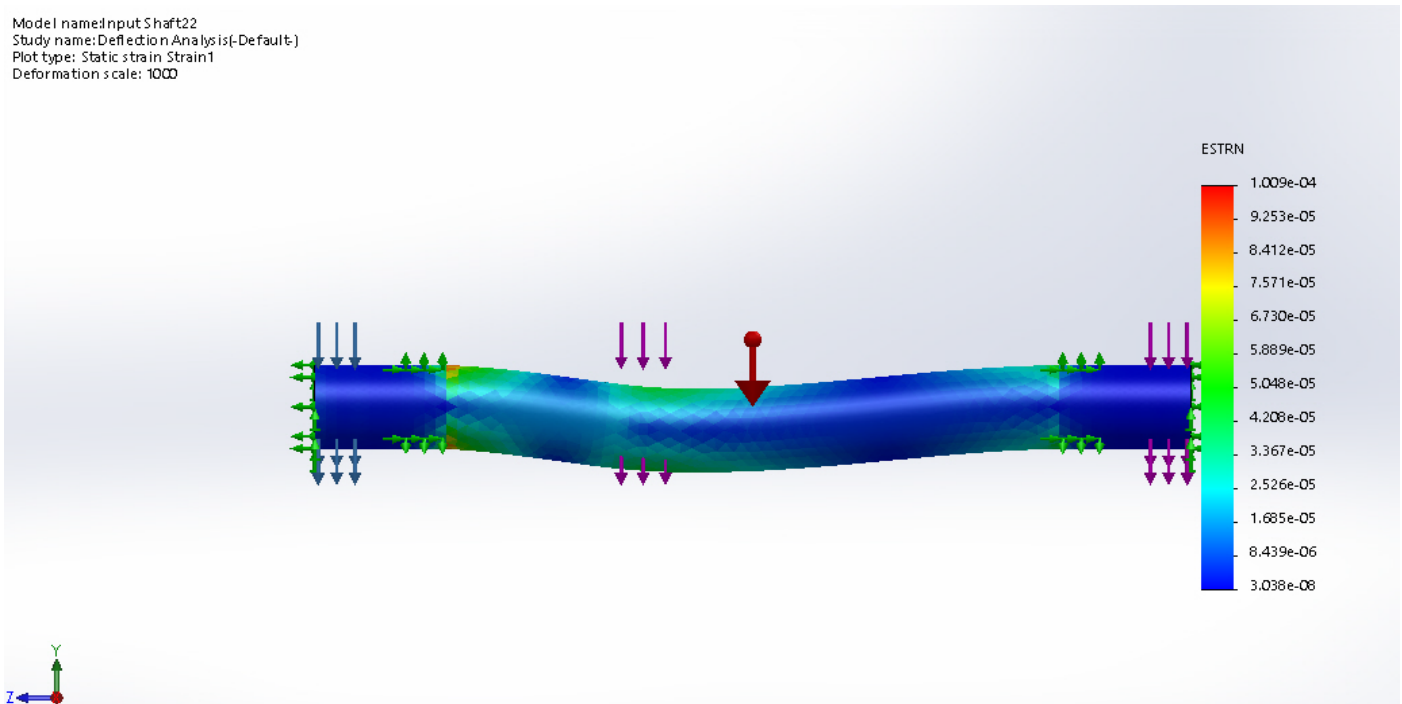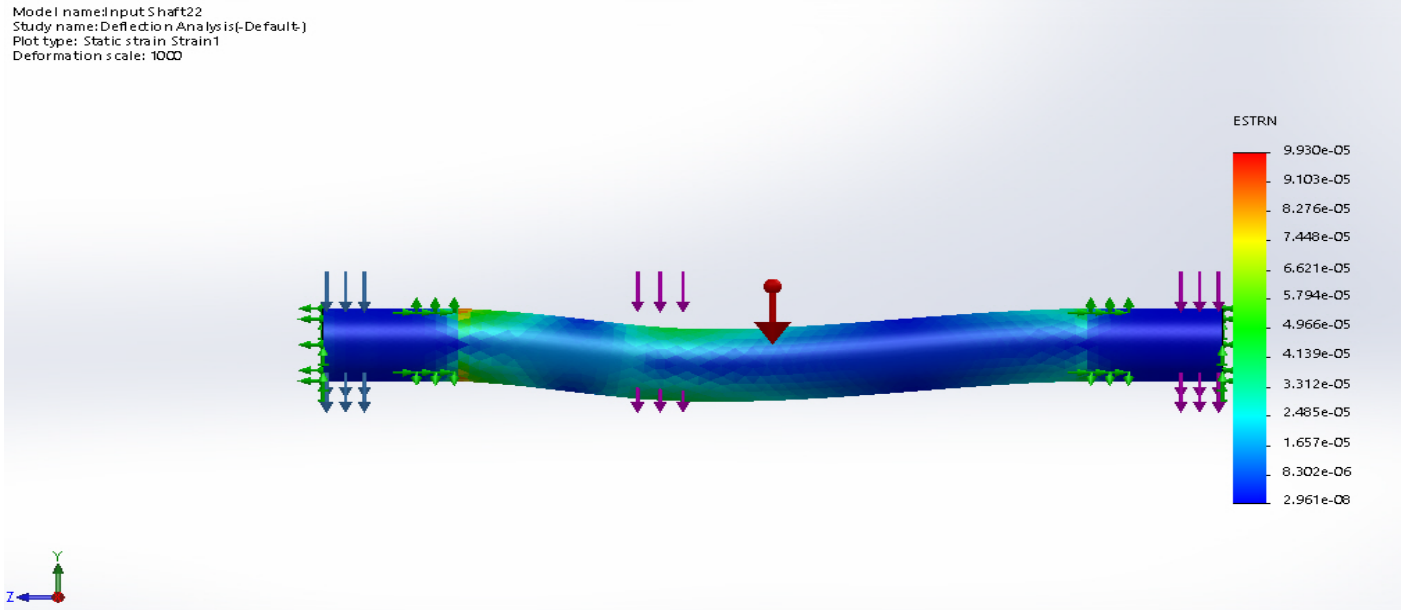**Fig 9a.** Static strain simulation plot for AISI 1020 steel (cold rolled)
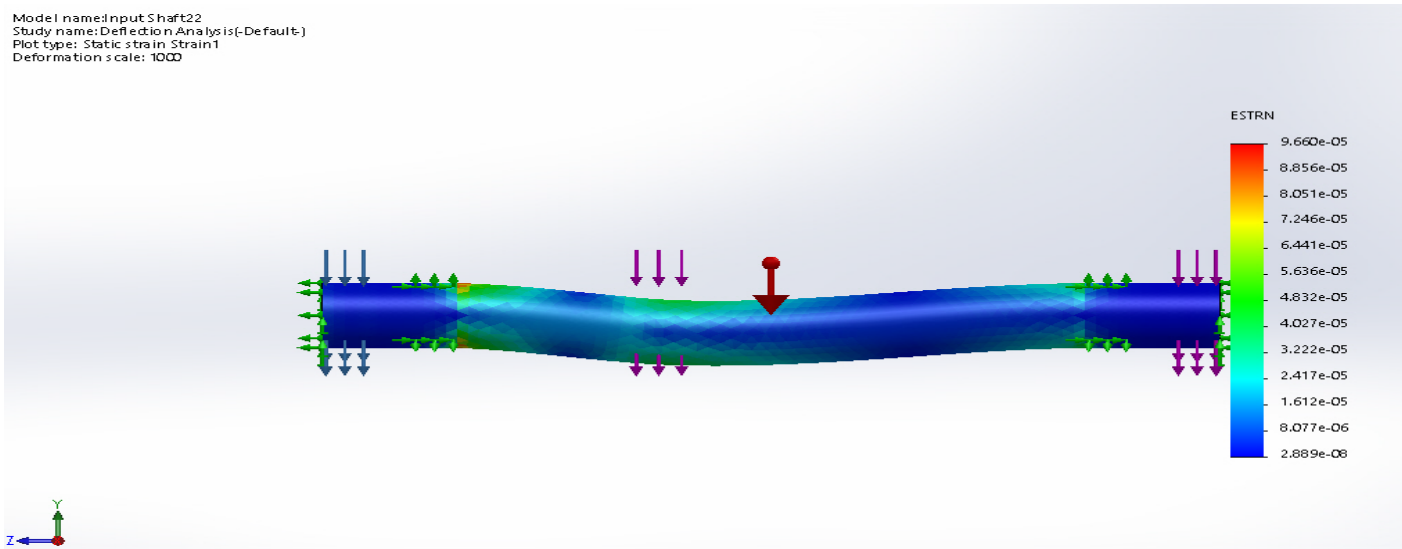

Fig 9b. Static strain simulation plot for cast carbon Steel

88

Fig 9c. Static strain simulation plot for cast carbon steel (cold rolled)

Fig 9d. Static strain simulation plot for AISI 4130 steel, annealed at $865^{o}C$

Maximum equivalent strain on each rotor sun gear shaft material extracted from the simulated plot in Figures 9a-d indicated that AISI 4130 steel (annealed at 865oC) possessed the minimum level of strain, followed by AISI 1020 steel (cold rolled), cast carbon steel (cold rolled) before cast carbon steel. Considering the relationship between static strain and FOS, it is possible that the rotor sun gear shaft material with the highest FOS will possess the least level of strain and vice versa. This is evidence in Figure 10 which clearly shows that AISI 4130 steel (annealed at 865oC) which had the highest FOS possess the minimum level of strain deformation while cast carbon steel which had the lowest FOS possessed the highest level of strain deformation. This therefore confirms that the failure of a given rotor sun gear shaft material with high FOS due to strain elastic deformation will be less and such material may not fail untimely during service condition and vice versa.
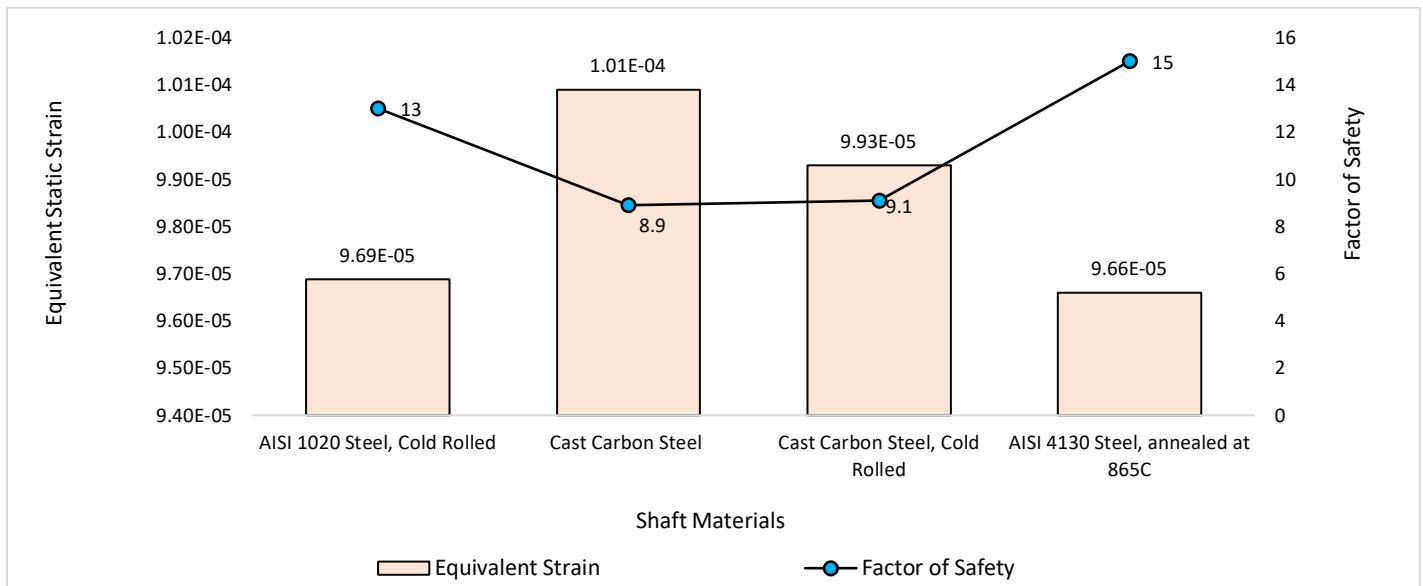
Fig 10. Graphical representation of equivalent static strain and FOS

4. Conclusion

The deflections undergone by four carbon steel materials used for statically loaded sun gear shaft of 2-stage planetary gear was analysed SOLIDWORKS 2018 version using FEM. The von-Mises stress produced by each material employed in the analysis did not exceed any of the material's yield their yield strength, and were found to occur within the design permissible limit. This lead to the conclusion that the materials are ductile in nature, and that they obeyed Hook's law of elasticity. Among the four materials analysed in this study, AISI 4130 steel: annealed at 865oC which possessed the highest FOS of 15 exhibited the highest strength value of 4.31E+08 MPa before failure. The other three materials also followed the same train in the order of their FOS. This lead to the conclusion that, the importance of FOS in the design of engineering components cannot be overemphasised. However, the selection of high FOS guarantees the safety of a given design, but it attracts higher cost that can be compensated for with the yield strength, optimum performance, longevity and above all, customer's preference which attracts high demand, application, recommendation and patronage.

References

[1] S. H. Loewenthal, "Design of Power Transmitting Shafts". Lewis Research Centre Cleveland, Ohio, NASA Reference Publication, 1123, 1984.

[2] P. Childs, "Mechanical Design Engineering Handbook". Butterworth-Heinemann, ISBN: 978-0-08-097759-1, 2014.

[3] E. V. Kumar, "Design and Analysis of Rotor Shaft Assembly of Hammer Mill Crusher". International Journal of Engineering and Management Research, 3(2), 22-30, 2013.

[4] M. Ramakotaiah, M. S. Kumar, T. R. Babu, and T. R. Teja, "Stress Analysis on a Turbine Shaft". International Journal of Engineering Research and Technology, 6(8), 394-397, 2017.

[5] R. A. Gujar, and S. V. Bhaskar, "Shaft Design under Fatigue Loading by Using Modified Goodman Method". International Journal of Engineering Research and Applications, 3(4), 1061-1066, 2013.

[6] N. L. Rakesh, V. Palanisamy, and S. Jeevabharathi, "Stress Analysis of a Shaft Using Ansys". Middle-East Journal of Scientific Research 12(12), 1726-1728, 2012.

[7] A. N. Eraslan, and T. Akis,"On the plane strain and plane stress solutions of functionally graded rotating solid shaft and solid disk problems". Acta Mechanica, 181, 43-63, 2006.

[8] K. Yoon, Y. Lee, and P. S. Lee, "A continuum mechanics based 3D beam finite element with warping displacements and its modelling capabilities", Struct. Eng. Mech. 43 (4), 411-437, 2012.

[9] J. Wang, V. V. Hurskainen, M. K. Matikainen, J. Sopanen, and A. Mikkola, "On the dynamic analysis of rotating

shafts using nonlinear super element and absolute nodal coordinate formulations", Adv. Mech. Eng. 9(11), 1–14, 2017.

[10] K. Yoon, and P. S. Lee, "Nonlinear performance of continuum mechanics based beam elements focusing on large twisting behaviours", Comput. Methods Appl. Mech. Eng, 281, 106-130, 2014.

[11] B. Bozorgmehri, V. Hurskainen, M. K. Matikainen, and A. Mikkola, "Dynamic analysis of rotating shafts using the absolute nodal coordinate formulation", Journal of Sound and Vibration, 453, 214-236, 2019.

[12] G. V. Drydale, "Design of Shafts for General Engineering Applications" School of Mechanical Engineering, University of New South Wales, 1978.

[13] A. N. Eraslan, and E. Arslan, "Plane Strain Analytical Solutions to Rotating Partially Plastic Graded Hollow Shafts". Turkish J. Eng. Env. Sci. 31, 273-288, 2007.

[14] R.Yongsheng, D. Qiyi, and Z. Xingqi, "1089. Modeling and dynamic analysis of rotating composite shaft". Journal of Vibroengineering, 15(4), 1790-1806, 2013.

[15] J. J. Yu, "Dynamic Analysis of Rotor-Bearing Systems Using Three-Dimensional Solid Finite Elements". University of Alberta, Edmonton, Alberta, 1997.

[16] R. G. Budynas, and J. K.Nisbett, "Shigleys", Mechanical Engineering Design, Eighth Edition, McGraw-Hill, New York, ISBN: 978-007-126896-7, 2008.

[17] A. E. Ikpe, I. Owunna, and P. O. Ebunilo, "Determining the Accuracy of Finite Element Analysis when Compared to Experimental". Journal of Robotics, Computer Vision and Graphics, 1(1), 12-20, 2016.

[18] E. M. Etuk , A. E. Ikpe, and A. U. Adoh, "Modelling and Analysis of 2-Stage Planetary Gear Train for Modular Horizontal Wind Turbine Application". Journal of Applied Research on Industrial Engineering, 6(4), 268-282, 2019.

[19] A. E. Ikpe and I. B. Owunna, "Design of Remotely Controlled Hydraulic Bottle Jack for Automobile Applications". International Journal of Engineering Research and Development, 11(1), 124-134, 2019.

[20] R. G. Ryan, "Using a Finite Element Stress Analysis Program to Enhance Learning In a Machine Design Course". California State University, Northridge, 2004.

[21] A. E. Ikpe, E. K. Orhorhoro, and A. Gobir, "Design and Reinforcement of a B-Pillar for Occupants Safety in Conventional Vehicle Applications". International Journal of Mathematical, Engineering and Management Sciences, 2(1), 37-52, 2017.

[22] A. E. Ikpe, , I. B. Owunna, and P. Satope, "Design optimization of a B-pillar for crashworthiness of vehicle side impact". Journal of Mechanical Engineering and Sciences, 11(2), 2693-2710, 2017.

[23] I. Owunna, , A. E. Ikpe, and J. I. Achebo, "Temperature and Time Dependent Analysis of Tungsten Inert Gas Welding of Low Carbon Steel Plate using Goldak Model Heat Source". Journal of Applied Science and Environmental Management, 22(11), 1719–1725, 2018.

[24] A. E. Ikpe, O E. Efe-Ononeme, and G. O. Ariavie, " Thermo-Structural Analysis of First Stage Gas Turbine Rotor Blade Materials for Optimum Service Performance". International Journal of Engineering & Applied Sciences, 10(2), 118-130, 2018.

[25] A. E. Ikpe, I.Owunna, , P. O. Ebunilo, and E. E. Ikpe, "Static Analysis on a Vehicle Tie Rod to Determine the Resulting Buckling Displacement". International Journal of Industrial and Manufacturing Systems Engineering, 1(1), 16-24, 2016.

[26] A. E. Ikpe, and I. Owunna, "Design of Vehicle Compression Springs for Optimum Performance in their Service Condition". International Journal of Engineering Research in Africa, 33, 22-34, 2017.

[27] A. P. Boresi, R. J. Schmidt, and O. M. Sidebottom, Advance Mechanics of Materials, Wiley, 1993.

[28] A. E. Ikpe, and I. B. Owunna, "Design Analysis of Reciprocating Piston for Single Cylinder Internal Combustion Engine". International Journal of Automotive Science and Technology, 4(2), 30-39, 2020.

[29] I. Owunna, A. Ikpe, , P. O. Ebunilo, and E. Ikpe, "Investigation of a vehicle tie rod failure in relation to the forces acting on the suspension system", American Journal of Engineering Research, 5(6), 208-217, 2016.